Corrosion Engineering, Science and Techno

# Geo-mapping atmospheric corrosion in Mauritius

| | |
|---|---|
| Journal: | *Corrosion Engineering, Science and Technology* |
| Manuscript ID | CES-24-0098.R1 |
| Manuscript Type: | Original Research Article |
| Date Submitted by the Author: | n/a |
| Complete List of Authors: | Seechurn, Yashwantraj; University of Mauritius,<br>Wharton, Julian; University of Southampton<br>Surnam, B. Yashwansingh R.; University of Mauritius |
| Keywords: | Atmospheric corrosion < Corrosion Phenomena, Carbon steel < Materials (substrates), Corrosion in marine environments < Corrosion Phenomena, Corrosion modelling < Techniques, Corrosion rate < Properties |
| Abstract: | The complexity of atmospheric corrosion prediction in Mauritius, due to the influence of trade winds and mountainous landscapes, presents a hurdle in building a more resilient infrastructural system. In the absence of a corrosion map, corrosion rate at a specific location is difficult to estimate. To achieve the UN Sustainable Development Goal 9 (Industry, Innovation and Infrastructure), an attempt is made to map the corrosivity of the whole country through regression modelling techniques and consideration of the factors affecting corrosion behaviour in the region. Previous field tests have recently been complemented with additional outdoor exposures to give a whole picture of the corrosivity of the Mauritian atmosphere. In this study, the relevant environmental data and known corrosion rates of carbon steel in specific locations are used to develop a corrosion map of the island as a vector data model depicting zones of specific ISO 9223 corrosivity categories. |
| | |

# Geo-mapping atmospheric corrosion in Mauritius

Yashwantraj Seechurn[a,b], Julian A. Wharton[b], Baboo Y. R. Surnam[a]

[a]*Mechanical and Production Engineering Department, Faculty of Engineering, University of Mauritius, Reduit 80837, Mauritius*
[b]*National Centre of Advanced Tribology at Southampton (nCATS), School of Engineering, University of Southampton, Southampton, SO17 1BJ, UK*

**Abstract**

The complexity of atmospheric corrosion prediction in Mauritius, due to the influence of trade winds and mountainous landscapes, presents a hurdle in building a more resilient infrastructural system. In the absence of a corrosion map, corrosion rate at a specific location is difficult to estimate. To achieve the UN Sustainable Development Goal 9 (Industry, Innovation and Infrastructure), an attempt is made to map the corrosivity of the whole country through regression modelling techniques and consideration of the factors affecting corrosion behaviour in the region. Previous field tests have recently been complemented with additional outdoor exposures to give a whole picture of the corrosivity of the Mauritian atmosphere. In this study, the relevant environmental data and known corrosion rates of carbon steel in specific locations are used to develop a corrosion map of the island as a vector data model depicting zones of specific ISO 9223 corrosivity categories.

*Keywords: Atmospheric corrosion; Carbon steel; Corrosion in marine environments; Corrosion modelling; Corrosion rate*

**Abstract**

The complexity of atmospheric corrosion prediction in Mauritius, due to the influence of trade winds and mountainous landscapes, presents a hurdle in building a more resilient infrastructural system. In the absence of a corrosion map, corrosion rate at a specific location is difficult to estimate. To achieve the UN Sustainable Development Goal 9 (Industry, Innovation and Infrastructure), an attempt is made to map the corrosivity of the whole country through regression modelling techniques and consideration of the factors affecting corrosion behaviour in the region. Previous field tests have recently been complemented with additional outdoor exposures to give a whole picture of the corrosivity of the Mauritian atmosphere. In this study, the relevant environmental data and known corrosion rates of carbon steel in specific locations are used to develop a corrosion map of the island as a vector data model depicting zones of specific ISO 9223 corrosivity categories.

*Keywords: Atmospheric corrosion; Carbon steel; Corrosion in marine environments; Corrosion modelling; Corrosion rate*

## 1. Introduction

Sustainable development is linked to infrastructure projects which are financially viable (1). And, reduction of the total costs incurred due to infrastructural corrosion damage requires adequate corrosion management. However, the latter is only effective with reliable prediction, which is a challenge for Small Island Development States (SIDS). With the growing awareness of the importance of infrastructure resilience, investment decisions are required to be evidence-based (1,2). Mauritius, a SIDS subtropical country with 1865 $km^2$ land area, is impacted by high humidity and dominant south-easterly trade winds that carry natural airborne sea particles onshore. The marine aerosols intercepted by the mountain ranges and high surf conditions in the absence of coral reefs along the south/southeast coast, illustrated in Figure 1, lead to a complex atmospheric distribution of chlorides across the island. Furthermore, gaseous emissions mainly from power stations in the capital, Port Louis (PL), give rise to a microclimate, with a high concentration of sulphur dioxide ($SO_2$). The latter plays an important role in increasing corrosion rate of steel infrastructure in industrial regions.

[insert Figure 1.]

Research on marine atmospheric corrosion in tropical regions has attracted interest from several researchers through the years. Atmospheric corrosion tests were performed in the Caribbean area comprising of Cuba, Mexico and Venezuela, all with a maritime climate (3). ISO 9223 corrosivity category as high as C5 for sites on the coastline, and decreasing corrosion kinetics with distance from the sea, were observed. To investigate the long-term corrosion of steel in Mauritius, corroded members of two bridges at varying distances (297 m and 770 m) from the sea, were examined. It was found that the top surfaces of the bridge closer to the sea had been more seriously damaged, confirming the reduced effect of chloride-induced corrosion with distance from the shore (4). When taking the seashore distance into account, it is also important to consider the direction of the wind, which influences the distance travelled by sea salts, produced as fine sprays from waves crashing on the shore (5). Thus, wave height data obtained from wave buoys in proximity to the test sites are very useful (6). In a study of marine atmospheric corrosion of mild steel in Spain, with samples facing the sea and the wind blowing from sea to land, the salinity level was found to be lower for the site nearer the coastline due to the presence of cliffs obstructing the flow of aerosol particles from the sea (7). Furthermore, a lower corrosion rate was obtained for the site with a higher chloride deposition rate, due to a lower dissolved oxygen level in the electrolyte formed on the surface. Nevertheless, there has been the general observation of atmospheric salt concentration being significant for a few hundred meters before a rapid decrease.

Recent field tests in PL (northwest – marine/industrial), Medine Camp de Masque (MC) (centre–rural), Fond du Sac (FS) (north-rural), Gris Gris (GG) (south-marine), La Gaulette (LG) (west-marine) and La Rosa (LR) (southeast-rural), shown in Figure 1, have given new insights on the corrosion behaviour of carbon steel in Mauritius (8–10). PL, LG and LR are at ISO category C2 while MC and FS are at ISO category C3. GG has the highest corrosivity, with the yearly corrosion rate lying in the CX ISO category. The corrosion rates in the east (rural) and centre (urban) locations are also available from previous studies (11,12). An urban site 13 km off the nearest coast (Vacoas), an eastern marine location 50 m from the shoreline (Belle Mare), and a rural site (Réduit) which is close to PL (9 km away) have all been associated with category C3 (medium) (11,12), analogous to that of the mid-island site (MC) and northern location (FS) 14 km and 6.5 km inland respectively. The similar corrosivity category for all these locations, of varying distances from the coast, shows that proximity with the shoreline does not necessarily lead to higher corrosion and high Time-of-Wetness (TOW) at the central locations is potentially the main cause of corrosion there.

Data collected from atmospheric corrosion exposure tests are normally used to find a relationship between the degradation of the metal and the environmental conditions, which would provide useful information on the progress of corrosion, especially during long periods of monitoring (13). Although the commonly used regression models are restricted in their capacity to represent the nonlinear corrosion behaviour, the use of regression equations to determine the influence of environmental parameters is very relevant (14). Crucial observations have been made with the use of this method e.g., to observe the relationship between average salinity and mean height of wave spectra (15). In an atmospheric corrosion study in Cuba, a regression showed the negligible influence of $SO_2$ concentration compared to chloride deposition rate based on the value of the coefficients (16). While $SO_2$ and chloride are the atmospheric pollutants most likely to cause an acceleration of corrosion, the humidity-temperature complex is also a key factor in the corrosion process and is considered by incorporating average yearly values of relative humidity and temperature as dependent parameters in a regression equation.
The fact that Mauritius shows a wide array of environmental conditions varying geographically, makes atmospheric

corrosion prediction quite complex. In this respect, corrosion rates displayed through maps are vital information for design and maintenance engineers who must ensure structures' durability in various service environments (17). A country corrosion map backed by a regression model can better facilitate the task of selecting material, protection systems, and maintenance intervals. Such a map is an example of an evidence-based tool which is vital for accurate assessment and proper planning of any infrastructure project (1,2).

## 2. Methodology

### *2.1. Field exposure*

S235 grade carbon steel plates of size 150 x 100 x 3 mm were exposed for up to two years at strategic locations around the island (FS, GG, LG, LR, MC and PL) as shown in Figure 1. The surfaces exposed at 45° to the horizontal in dedicated racks (8,9) (Figure 2).

[insert Figure 2.]

### *2.2. Regression Modelling*

Multiple Regression Modelling is used to obtain an equation for the corrosion rate ($r_{corr}$), which is the dependent parameter, as a function of the relevant independent parameters: atmospheric concentration of sulphur dioxide – $[SO_2]$ / mg m$^{-2}$ d$^{-1}$, chloride deposition rate – *CDR* / mg m$^{-2}$ d$^{-1}$, relative humidity – *RH* / % and temperature – *T* / °C.

In (9) and (8), the corrosion rates have been calculated from data obtained within one year of exposure. However, for a more accurate prediction of corrosion rate, this study uses data from samples exposed up to 24 months (Appendix A). Removal of the weathered plates were carried out at various time points during the test period and subsequently subjected to chemical cleaning according to ISO 8407 (18). This procedure was repeated multiple times to ensure removal of all traces of rust such that the mass loss could be taken. The corrosion rate for each test location, calculated as per Eqn. 1, was then used to assign corrosivity classification according to the standard categories defined in ISO 9223 (19). The total attack (*D*) defined as the mass loss per m$^2$ (20) was also obtained as a linear or power function of t (Eqn. 2 or Eqn. 3, whichever gives the higher $R^2$ value) to obtain $r_{corr}$ for a specific time of exposure. $[SO_2]$ and *CDR* were measured using the sulfation plate and wet candle method respectively, as per ISO 9225 (21).

$$r_{corr} = \frac{\Delta m}{A \cdot t} \quad (1)$$

where $r_{corr}$ is the corrosion rate in g m$^{-2}$ y$^{-1}$, $\Delta m$ is the mass loss in g, $A$ is the surface area in m$^2$, $t$ is the exposure time in years (y).

$$D = r_{cor} t^b \quad (2)$$

where $b$ is a constant.

$$D = a r_{corr} + c \quad (3)$$

where $a$ and $c$ are constants.

A multiple linear regression model fitting the independent variables *T*, *RH*, *CDR* and $[SO_2]$ is in the following form:

$$r_{corr} = \beta_0 + \beta_1 T + \beta_2 RH + \beta_3 CDR + \beta_4 [SO_2]$$

where $\beta_0$ is the y-intercept and $\beta_1$,$\beta_2$,$\beta_3$,and $\beta_4$ are the coefficients.

The total Degree of Freedom (DF) is four and this model can be used to analyse the effect of more than one independent parameter on the corrosion rate (dependent variable).

### 2.3. Corrosion mapping

Using ArcMap 10.8, a tool in ArcGIS software, the corrosion map is developed as a vector data model. This geostatistical analysis tool is effective in organizing geographic data and constructing maps to visualize any spatial distribution (22). The various zones of corrosivity classification are discrete entities represented by spatial features (polygons from a vector point of view) (23). Polygon is a vector primitive, which is the building block used in the vector data model. Boundaries are drawn stepwise, taking into account the relevant pollution factors, environmental parameters and landforms influencing corrosion in the country.

## 3. Results and Discussions

### 3.1. Multiple Regression Analysis

Table 1 lists the data for all environmental parameters (independent) at the different sites and the corresponding corrosion rates (dependent) used to fit the multiple linear regression model. The linear or power law equation of *D vs*. *t*, obtained from the measured mass loss data at the various timepoints, was used to determine the $r_{corr}$ at exactly two years at each test site. Regarding PL, average values have been considered since various sites (AM, FG, FV, LM, MA and RG) within 1.8 km were investigated in this region (8), except for temperature and relative humidity data which are common to all the PL locations. The data for each independent variable (*T*, *RH*, *CDR* and [$SO_2$], are average values calculated from data measured over the period over which the field exposures were carried out.

**Table 1.** Environmental parameters and corrosion rates obtained at the Mauritius test sites.

| Site | | *T* / °C | *RH* / % | *CDR* / mg m$^{-2}$ d$^{-1}$ | | [$SO_2$] / mg m$^{-2}$ d$^{-1}$ | | Corrosion Equation | $R^2$ | $r_{corr}$ / g m$^{-2}$ y$^{-1}$ | |
|---|---|---|---|---|---|---|---|---|---|---|---|
| FS | | 24.8 | 77 | 214.6 | | 1.93 | | $D = 155.66t + 74.545$ | 0.9929 | 230.2 | |
| GG | | 25.3 | 77 | 1766.0 | | 0.59 | | $D = 4390.9t - 678.73$ | 0.9923 | 3712.2 | |
| LG | | 25.6 | 72 | 59.7 | | 1.54 | | $D = 101.95t^{0.41}$ | 0.994 | 102.0 | |
| LR | | 24.7 | 78 | 126.2 | | 1.45 | | $D = 192.25t^{0.57}$ | 0.999 | 192.3 | |
| MC | | 24.2 | 75 | 71.5 | | 1.17 | | $D = 150.8t + 56.894$ | 0.9874 | 207.7 | |
| PL | AM | 26.4 | 68 | 31.5 | 31.3 | 1.39 | 1.60 | $D = 70.559t + 41.703$ | 0.9927 | 112.3 | 130.3 |
| | FG | | | 41.6 | | 1.90 | | $D = 86.155t + 98.823$ | 0.9586 | 185.0 | |
| | FV | | | 31.2 | | 2.37 | | $D = 110.42t + 69.118$ | 0.9621 | 179.5 | |
| | LM | | | 11.4 | | 1.16 | | $D = 109.12t^{0.56}$ | 0.9976 | 109.1 | |
| | MA | | | 14.5 | | 1.36 | | $D = 48.252t + 28.938$ | 0.993 | 77.2 | |
| | RG | | | 57.3 | | 1.43 | | $D = 71.238t + 47.215$ | 0.9873 | 118.5 | |

### 3.2. t-test

A t-test is performed for each regression coefficient. The null and alternative hypotheses are as follows:

$$H_0: \beta_i = 0$$
$$H_\alpha: \beta_i \neq 0$$

At 95% confidence level for parameters, the null hypothesis is rejected when the *p*-value is less than 0.05. Table 2 shows that the *p*-value for all parameters is greater than 0.05 except for *CDR*. Therefore, the null hypothesis is not rejected for the coefficients of *RH*, [$SO_2$] and *T* implying that there is no statistical significance for these parameters.

**Table 2.** Multiple Regression parameters.

| | Value | Standard Error | t-value | Prob>\|t\| |
|---|---|---|---|---|
| Intercept | 1344.452 | 1726.072 | 0.77891 | 0.57872 |
| *CDR* | 1.98282 | 0.05466 | 36.27873 | 0.01754 |
| *RH* | -15.0992 | 9.5286 | -1.58463 | 0.35838 |
| [$SO_2$] | -309.522 | 62.410 | -4.95949 | 0.12667 |
| *T* | 8.82298 | 44.54270 | 0.19808 | 0.87551 |

*3.3. F-test*

An F-Test is carried out:

Null hypothesis: There is equal fit of the model obtained and an intercept-only model
Alternative Hypothesis: The fit observed from the intercept-only model is markedly inferior to the multivariate model

Since the *p*-value obtained from the F-test (Table 3) is less than 0.05 (significance level), the null hypothesis is rejected thereby confirming that the model with all the independent variables is better than the intercept-only model.

**Table 3.** ANOVA of corrosion rate and environmental parameters.

| | DF | Sum of Squares | Mean Square | F value | Prob>F |
|---|---|---|---|---|---|
| Model | 4 | 1.05E+07 | 2630336 | 3573.081 | 0.01255 |
| Error | 1 | 736.1534 | 736.1534 | | |
| Total | 5 | 1.05E+07 | | | |

*3.4. Linear Regression Analysis*

Based on the results of the t-test and F-test following a multiple regression analysis, it is deemed more appropriate to carry out a linear fitting with only *CDR* as the independent variable. The results are shown in Table 4.

**Table 4.** Linear Regression Parameters.

| | Value | Standard Error | t-value | Prob>\|t\| |
|---|---|---|---|---|
| Intercept | -36.8323 | 56.50385 | -0.65185 | 0.55005 |
| Slope | 2.11845 | 0.07749 | 27.33922 | 1.06E-05 |

The *p*-value for the slope coefficient is less than 0.05 which implies the null hypothesis may be rejected. A $R^2$ of 0.995 infers that the corrosion rates are well explained with changes in *CDR* by a linear equation (Eqn. 2).

$$r_{\text{corr}} = 2.12\ CDR - 36.8 \quad (2)$$

The normality plot of the residuals (Figure 3) shows the data points evenly distributed about the regression line, thereby confirming the validity of the regression model.

[insert Figure 3.]

### *3.5. Chloride ion diffusion model*

In the PL region the wind direction is generally west/northwest, *i.e.*, the wind direction is from land to sea. Therefore, the exposed specimen surfaces are facing the sea but on the downwind side. Furthermore, the PL region is protected from wind-blown marine aerosols and salts from the south/east sea by the Moka mountain range (Figure 1). Similarly, LG is shielded by the Black River and Savanne mountain ranges (Figure 1). This explains the low *CDR* at these locations (Table 1), despite their proximity to the shoreline. The barrier effect is reduced for mountains with gentle slopes (24), however, the Mauritius mountain ranges are very steep, resembling thin walls (25) and therefore provide a chloride-free zone on the downwind side. The relative humidity in the western regions is also significantly lower compared to other parts of the island. In this study, the inland atmospheres (MC, LR and FS), have salinity levels due to ocean-generated sea aerosol (26), which are higher than that at LG and the PL average. Therefore, *CDR* cannot be considered as a decreasing function of seashore distance unless a relationship of *CDR* variation with distance is obtained by taking distance from the east/south shore only up to locations where the mountain ranges are not blocking the path of sea salts travel. Since GG, LR, MC and FS fulfil this criterion, the corresponding chloride deposition rates and distances for these locations are used (Table 5) and a power law relationship between *CDR* and seashore distance is obtained as shown in Figure 4. The latter indicates a rapid fall-off in *CDR* given that the salinity at GG is mainly due to surf-generated aerosol and the source of chlorides at the other locations are ocean whitecaps (27).

**Table 5.** Shore distance and Chloride deposition rate.

| Test Site | Distance from the east or south shore / km | *CDR* / mg m$^{-2}$ d$^{-1}$ |
|---|---|---|
| GG | 0.02 | 1766.0 |
| FS | 6.5 | 214.6 |
| LR | 7.8 | 126.2 |
| MC | 13.9 | 71.5 |

[insert Figure 4.]

The $R^2$ value of 0.997 shows that the graph fits the data well. Therefore, knowledge of the distance from the seashore can provide a good estimation of salinity level in the absence of any major interfering landform such as a mountain range.

The power law equation is:

$$CDR = 345.9s^{-0.42} \quad (3)$$

where $s$ is the distance from the shore.

Wind generally blows from a south-easterly direction on the island and as a result, deposition of marine salts occurs predominantly in the southeast coastal locations. Since *CDR* is known to decrease with distance from the coast (28), salinity is expected to be lower further inland and the west coast is almost entirely protected from the wind-blown aerosols due to the presence of the mountain ranges. The graphical relationship of *CDR vs. s* for the windward side of the mountain range, therefore, gives a useful indication of the rate at which salinity decreases over long distances.

### *3.6. Corrosion Mapping*

#### *3.6.1. Step 1*

By combining Eqns. 2 and 3, an equation for $r_{corr}$ as a function of the distance from the shore ($s$) is obtained (Eqn. 4). From ISO 9223 (19), each corrosivity category (C1, C2, C3, C4, C5 and CX) is associated with a range of corrosion rate values, and Table 6 lists the distance from the sea up to which any specific category prevails, for conditions specific to Mauritius, calculated using Eqn. 4. As illustrated in Figure 5, a preliminary corrosion map is then obtained by defining boundaries from the east/south coast with respect to the distances from Table 6, and also considering the

location of the mountain ranges.

$$r_{\text{corr}} = 733.3s^{-0.42} - 36.8 \quad (4)$$

**Table 6.** Corrosivity Category coverage over specific distances.

| ISO 9223 Corrosivity Category | $r_{\text{corr}}$ / g m$^{-2}$ y$^{-1}$ | $s$ / km |
|---|---|---|
| CX - Extreme | >1500 | 0.17 |
| C5 – Very High | 650-1500 | 1.17 |
| C4 - High | 400-650 | 3.43 |
| C3 - Medium | 200-400 | 14.8 |
| C2 - Low | <10 | 700 |

[insert Figure 5.]

*3.6.2. Step 2*

Locations up to 1 km from the coast are likely to be within an area of significant chloride activity (26). However, Table 6 shows that high corrosivity is present up to 3.43 km from the east/south shore of Mauritius, with the main source of salts originating from the coastal surf. Corel reefs are effective barriers in reducing the deposition of marine salts (29) and the absence of reefs along a length of the coast from the south to the southeast as observed in Figure 1, which includes Gris-Gris, causes waves breakage at the rocky shore leading to a corrosivity of the highest category (CX) existing closer to the coastline. Nonetheless, part of the south coast and most of the east coast are expected to have a low airborne salinity given the coral reefs are far (up to around 5 km) from the shore, resulting in reduced surf conditions (11). A previous study performed at Belle Mare (50 m from the east shoreline) showed that this region has a corrosivity in the C3 category (11). Thus, major lengths on the east and south coast, with lagoons, are attributed a corrosivity of the C3 category instead of a progressive reduction of corrosivity from CX to C4.

Therefore, the full effect of the southeast trade winds blowing marine salts is observed for coastal regions with no coral reefs and unprotected by the mountains. Coral reefs 500 m from the seashore do not have any impact on corrosion rate at the nearest coast as observed for the site at Belle mare. Similarly, a low corrosion rate is observed region wide in the western half of the island irrespective of distance from the mountains.

*3.6.3. Step 3*

Westward there is a decrease in corrosion rate down to the C2 category, except a rise in corrosion in the central regions, such as Medine Camp de Masque (MC) with a C3 corrosivity, attributable to its high RH (75%) (Table 1). Previous studies in Mauritius have shown that medium corrosivity C3 is observed in other mid-island locations such as Réduit and Vacoas, which are associated with high *RH* (75-90%), the latter being a major contributor to atmospheric corrosion in the island (11,12). The long-term climatic data, obtained from the Mauritius Meteorological Services, shows that February is one of the most humid months on the island. Therefore, an area representative of regions having *RH* greater than 75%, obtained from a relative humidity map of February 2022 (30), is superimposed on the preliminary map (Figure 5) and associated with corrosivity category C3. This causes the medium corrosivity region to extend beyond 14.8 km (predicted using Eqn. 4 and listed in Table 6) and further to the left.

*3.6.4. Step 4*

The western part of Mauritius is well shielded against the trade winds by the mountain ranges and receives favourable wind that blows from inland to the coast, leading to low corrosivity. Port-Louis can be attributed to a general corrosivity category of C2 except for the area downwind and at a distance of about 200 m from the stacks at Fort-George Power Station where higher corrosion rates exist as a result of deposition of pollutants from sulphur dioxide plume dispersion (31). Based on ISO 9223, the C3 and C4 regions shown in Figure 6, were mapped as per the $SO_2$

content displayed through a map of air quality for Fort George (31).

[insert Figure 6.]

A combination of factors has been shown to influence corrosion rate: coral reefs, RH and $SO_2$. The corrosion map of Mauritius, illustrated in Figure 7, is obtained based on Step 1 to Step 4 in the modelling process. The harsh marine conditions prevailing at GG explain the extreme corrosivity along the south/southeast coast.

[insert Figure 7.]

## 4. Conclusions

In the current study, chloride deposition rates from field exposures at Port-Louis (northwest–industrial), Medine Camp de Masque (centre–rural), Gris-Gris (south-rural), La Gaulette (west-rural), Fond-du-sac (north-rural) and La Rosa (southeast-rural) have been used to determine the spread of chlorides in Mauritius. The key insights gained for the country are as follows:

1. The first-year corrosion rates at these locations and similar data for some east-coast and mid-island locations, obtained from previous studies, contributed greatly to the development of a corrosion map. The latter will provide an improved understanding of atmospheric corrosivity throughout the country. Effective corrosion prevention measures could be taken which will lead to better maintenance of infrastructures, thereby ensuring durability, safety and reliability. Eventually, the cost of corrosion will decrease significantly, which is beneficial to the country in the medium and long term.

2. The results show a general trend of reduced $Cl^-$ deposition rate with a corresponding decrease in corrosion rate provided the path of travelling sea salt aerosols is unimpeded. The corrosion map, backed up by regression analysis and developed as a vector data model shows a decrease in corrosion rate westward from C3 down to the C2 category with the west coast well protected from the southeast trade winds by the mountain ranges. Therefore, expensive anti-corrosion coatings are generally not recommended for coastal infrastructure projects in the west.

3. The atmospheric concentration of sulphur dioxide is generally very low, except in the vicinity of the oil-fired power stations. The latter being a major source of pollution, $SO_2$ data there has not been used in obtaining the generalised multiple linear regression model. According to ISO 9223, the corrosivity category of an area can be estimated from the $SO_2$ content in that particular atmospheric environment. High corrosivity in Port Louis exists at 200 m downwind of Fort-George power station due to the deposition of plumes causing elevated $SO_2$ levels. Therefore, improved regulations on gas emissions, especially from oil-fired power stations, would help in significantly reducing the adverse effects of $SO_2$ on metal degradation.

4. Large parts of the east coast have low airborne salinity due to the coral reefs offering protection from breakers arriving near the seashore. With the exception of the southeast area where the unprotected waters lead to huge coastal waves increasing the aggressiveness of the atmosphere considerably. Effective strategies in the corrosion management of structures will lead to the development of sustainable infrastructure in aggressive atmospheres, thereby contributing to the economic development of Mauritius.

**Acknowledgements**

**Author contributions**

**Declaration of conflicting interest**

The authors declared no potential conflicts of interest with respect to the research, authorship, and/or publication of this article.

**References**


1. Adeoti T, Fantini C, Morgan G, O' CS, Regan N. Infrastructure for Small Island Developing States The role of infrastructure in enabling sustainable, resilient and inclusive development in SIDS [Internet]. 2020. Available from: www.unops.org

2. Adshead D, Román García O, Thacker S, Hall JW. Infrastructure Strategies for Achieving the Global Development Agendas in Small Islands. Earths Future. 2021 Feb 1;9(2).

3. Corvo F, Haces C, Betancourt N, Maldonado L, Véleva L, Echeverria M, et al. Atmospheric corrosivity in the Caribbean area. Corros Sci. 1997;39(5):823–33.

4. Surnam BYR, Katim MH. Corrosion in Bridges in Mauritius. In: CORCON. New Delhi; 2013.

5. Alcántara J, de la Fuente D, Chico B, Simancas J, Díaz I, Morcillo M. Marine atmospheric corrosion of carbon steel: A review. Materials. 2017;10(4).

6. Morcillo M, Chico B, Alcántara J, Díaz I, Simancas J, De La Fuente D. Atmospheric corrosion of mild steel in chloride-rich environments. Questions to be answered. Materials and Corrosion. 2015;66(9):882–92.

7. Morcillo M, Chico B, Mariaca L, Otero E. Salinity in marine atmospheric corrosion: Its dependence on the wind regime existing in the site. Corros Sci. 2000;42(1):91–104.

8. Seechurn Y, Wharton JA, Surnam BYR. Mechanistic modelling of atmospheric corrosion of carbon steel in Port-Louis by electrochemical characterisation of rust layers. Mater Chem Phys. 2022;291(April):126694.

9. Seechurn Y, Surnam BYR, Wharton JA. Marine atmospheric corrosion of carbon steel in the tropical microclimate of Port Louis. Materials and Corrosion. 2022;(October 2021).

10. Seechurn Y, Surnam BYR, Wharton JA. Marine atmospheric corrosion of carbon steel in Mauritius. Mater Today Proc. 2023;(July).

11. Surnam BYR. Three years outdoor exposure of low carbon steel in Mauritius. Anti-Corrosion Methods and Materials. 2015;62(4):246–52.

12. Surnam BYR, Oleti C V. Atmospheric corrosion in Mauritius. Corrosion Engineering Science and Technology. 2012;47(6):446–55.

13. Ma Y, Li Y, Wang F. The atmospheric corrosion kinetics of low carbon steel in a tropical marine environment. Corros Sci. 2010;52(5):1796–800.

14. Guerra JC, Castañeda A, Corvo F, Howland JJ, Rodríguez J. Atmospheric corrosion of low carbon steel in a coastal zone of Ecuador: Anomalous behavior of chloride deposition versus distance from the sea. Materials and Corrosion. 2019;70(3):444–60.

15. Alcántara J, de la Fuente D, Chico B, Simancas J, Díaz I, Morcillo M. Marine atmospheric corrosion of carbon steel: A review. Materials. 2017;10(4).

16. Corvo Perez F. Atmospheric corrosion of steel in a humid tropical climate - influence of pollution, humidity, temperature, solar radiation and rainfall. Corrosion. 1984;40(4):170–5.

17. Ivaskova M, Kotes P, Brodnan M. Air pollution as an important factor in construction materials deterioration in Slovak Republic. Procedia Eng. 2015;108:131–8.

18. BS EN ISO 8407. Corrosion of metals and alloys - Removal of corrosion products from corrosion test

specimens. BSI Standards Limited; 2014.

19. BS EN ISO 9223. Corrosion of metals and alloys — Corrosivity of atmospheres — Classification , determination and estimation. BSI Standards Limited; 2012. 26 p.

20. BS EN ISO 9224. Corrosion of metals and alloys — Corrosivity of atmospheres — Guidance values for the corrosvity categories. BSI Standards Limited; 2012.

21. BS EN ISO 9225. Corrosion of metals and alloys — Corrosivity of atmospheres — Measurement of environmental parameters. BSI Standards Pubilication. BSI Standards Limited; 2012.

22. Santa AC, Tamayo JA, Correa CD, Gómez MA, Castaño JG, Baena LM. Atmospheric corrosion maps as a tool for designing and maintaining building materials: A review. Vol. 8, Heliyon. Elsevier Ltd; 2022.

23. Brown DG, Riolo R, Robinson DT, North M, Rand W. Spatial process and data models: Toward integration of agent-based models and GIS. J Geogr Syst. 2005;7(1):25–47.

24. Cole IS, Chan WY, Trinidad GS, Paterson DA. Holistic model for atmospheric corrosion part 4 - Geographic information system for predicting airborne salinity. Corrosion Engineering Science and Technology. 2004;39(1):89–96.

25. Major H. de Haga Haig. The Physical Features and Geology of Mauritius. Quarterly Journal of the Geological Society. 1985;51(1–4).

26. Cole IS, Paterson DA, Ganther WD. Holistic model for atmospheric corrosion Part 1 - Theoretical framework for production, transportation and deposition of marine salts. Corrosion Engineering Science and Technology. 2003;38(2):129–34.

27. Cole IS, Ganther WD, Paterson DA, King GA, Furman SA, Lau D. Holistic model for atmospheric corrosion Part 2 - Experimental measurement of deposition of marine salts in a number of long range studies. Corrosion Engineering Science and Technology. 2003;38(4):259–66.

28. Hao W, Xu L, Chen X, Jin Y, Han Y, Zhang X, et al. Classification and spatial mapping of atmospheric corrosion of China. Npj Mater Degrad. 2022;6(1):1–8.

29. Cole IS, Paterson DA, Ganther WD, Neufeld A, Hinton B, McAdam G, et al. Holistic model for atmospheric corrosion Part 3 - Effect of natural and man made landforms on deposition of marine salts in Australia and south-east Asia. Corrosion Engineering Science and Technology. 2003;38(4):267–74.

30. Climate of Mauritius - Mauritius Meteorological Services [Internet]. [cited 2021 Jun 18]. Available from: http://metservice.intnet.mu/climate-services/climate-of-mauritius.php

31. Tatayah P. Air Quality - Fort George, Mauritius. 2017.

## Appendix A.

Table A.1. First-year mass loss data for S235 grade structural steel.

| Site | 1st removal | | | 2nd removal | | | 3rd removal | | | 4th removal | | |
|---|---|---|---|---|---|---|---|---|---|---|---|---|
| | *t* / y | Mass loss / g | STD. DEV | *t* / y | Mass loss / g | STD. DEV | *t* / y | Mass loss / g | STD. DEV | *t* /y | Mass loss / g | STD. DEV |
| FV | 0.17 | 2.711 | 0.125 | 0.42 | 4.096 | 0.106 | 0.68 | 4.797 | 0.314 | 0.96 | 5.153 | 0.080 |
| RG | 0.17 | 1.753 | 0.014 | 0.42 | 2.476 | 0.176 | 0.67 | 2.916 | 0.008 | 0.96 | 3.654 | 0.112 |
| LM | 0.17 | 1.256 | 0.052 | 0.42 | 2.113 | 0.203 | 0.67 | 2.829 | 0.139 | 1.17 | 3.833 | 0.186 |
| FG | 0.17 | 3.101 | 0.743 | 0.42 | 4.882 | 0.097 | 0.67 | 5.065 | 0.050 | 0.96 | 5.493 | 0.214 |
| MA | 0.18 | 1.156 | 0.031 | 0.42 | 1.550 | 0.110 | 0.67 | 1.895 | 0.070 | 0.96 | 2.330 | 0.138 |
| GG | 0.18 | 10.378 | 0.250 | 0.42 | 24.857 | 3.978 | 0.68 | 82.150 | 6.709 | 0.95 | 108.986 | 15.790 |
| MC | 0.18 | 2.469 | 0.175 | 0.43 | 3.858 | 0.093 | 0.67 | 5.098 | 0.264 | 0.95 | 6.824 | 0.646 |
| AM | 0.17 | 1.765 | 0.137 | 0.42 | 2.186 | 0.159 | 0.67 | 2.671 | 0.099 | 0.94 | 3.361 | 0.083 |
| FS | 0.17 | 3.235 | 0.121 | 0.42 | 4.492 | 0.245 | 0.78 | 5.906 | 0.056 | 1.24 | 8.574 | 0.433 |
| LG | 0.18 | 1.568 | 0.049 | 0.42 | 2.223 | 0.095 | 0.68 | 2.683 | 0.024 | 0.83 | 3.035 | 0.129 |
| LR | 0.18 | 2.247 | 0.094 | 0.42 | 3.753 | 0.137 | 0.66 | 4.782 | 0.289 | 1.07 | 6.242 | 0.682 |

Table A.2. Second-year mass loss data for S235 grade structural steel.

| Site | 5th removal | | | 6th removal | | |
|---|---|---|---|---|---|---|
| | *t* / y | Mass loss / g | STD. DEV | *t* / y | Mass loss (g) | STD DEV |
| FV | 1.2 | 5.770 | 0.079 | 2.0 | 9.690 | 0.783 |
| RG | 1.2 | 4.549 | 0.170 | 2.0 | 5.899 | 0.607 |
| LM | 2.0 | 4.942 | 0.540 | _ | _ | _ |
| FG | 1.2 | 6.324 | 0.121 | 2.0 | 8.671 | 0.576 |
| MA | 1.2 | 2.933 | 0.021 | 2.0 | 3.930 | 0.068 |
| MC | 1.2 | 6.903 | 0.106 | 2.0 | 11.424 | 1.107 |
| AM | 1.2 | 4.135 | 0.104 | 2.0 | 5.729 | 0.117 |

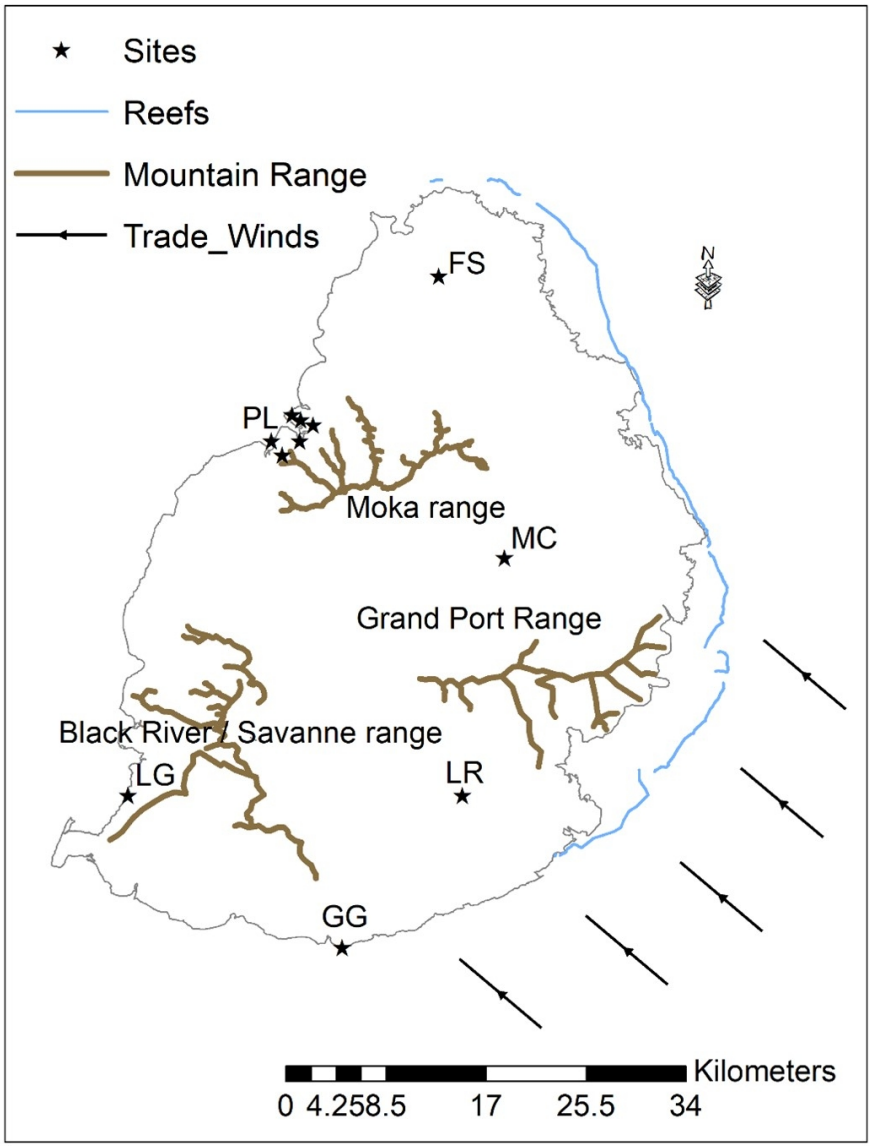


Figure 1. Map of Mauritius showing the test sites, mountain ranges, trade winds and coral reefs.

126x164mm (220 x 220 DPI)

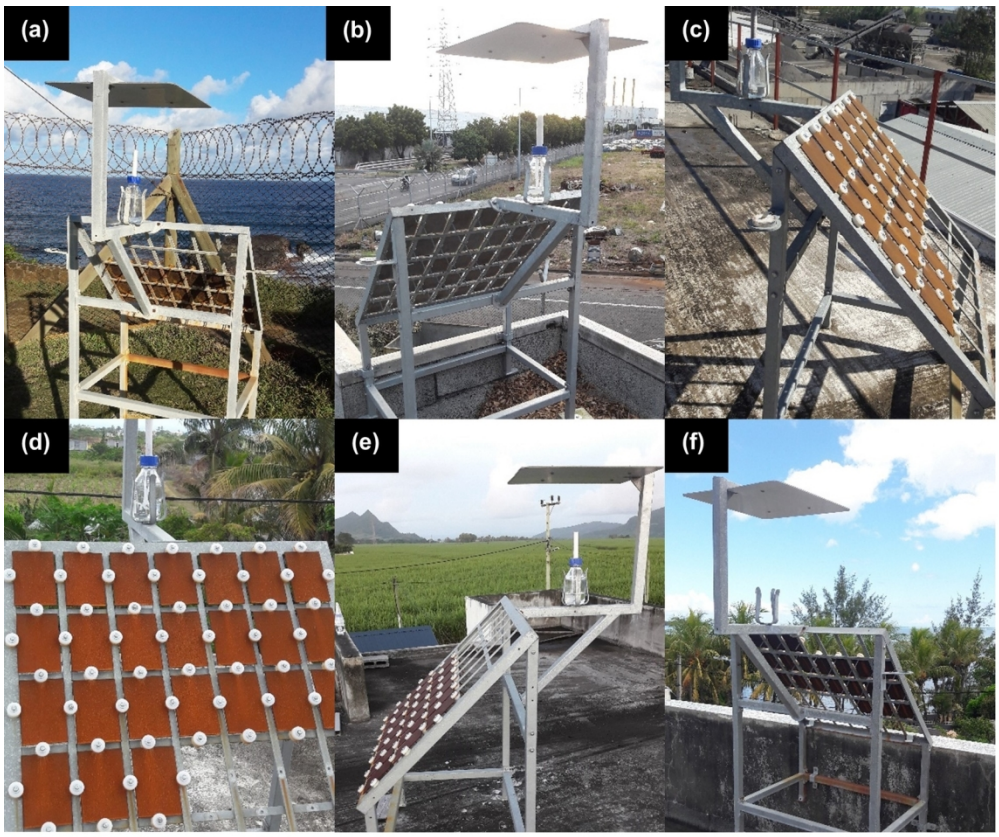


Figure 2. S235 grade carbon steel specimens on exposure racks at selected test sites: (a) Gris Gris (b) Port Louis (c) Fond du Sac (d) La Rosa (e) Medine Camp de Masque (f) La Gaulette.

150x125mm (300 x 300 DPI)

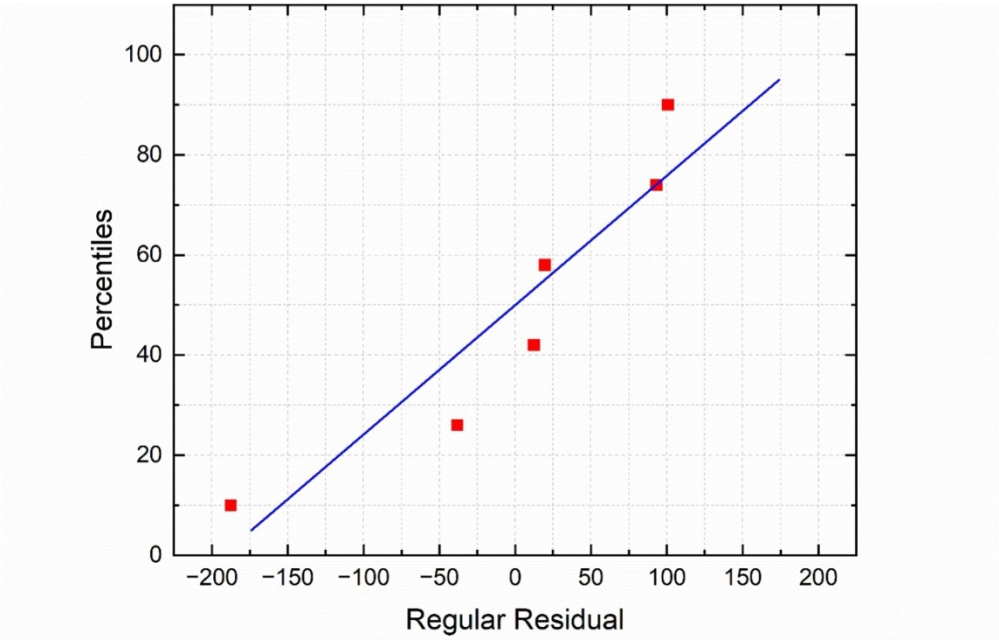


Figure 3. Regular Residual of Linear Fit with rcorr as the response and CDR as the predictor.

149x95mm (220 x 220 DPI)

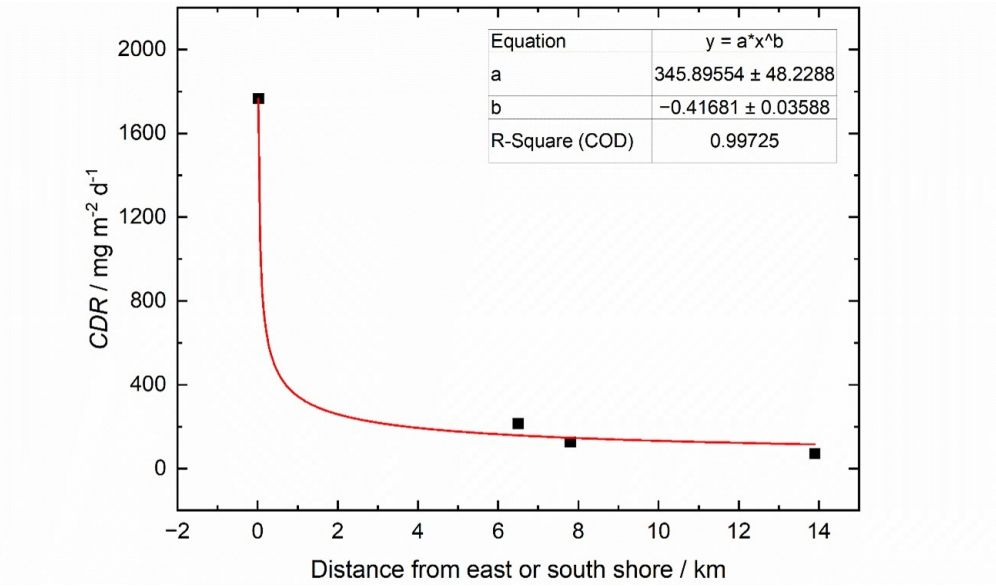


Figure 4. Variation of chloride deposition rate with distance from the sea.

149x87mm (220 x 220 DPI)

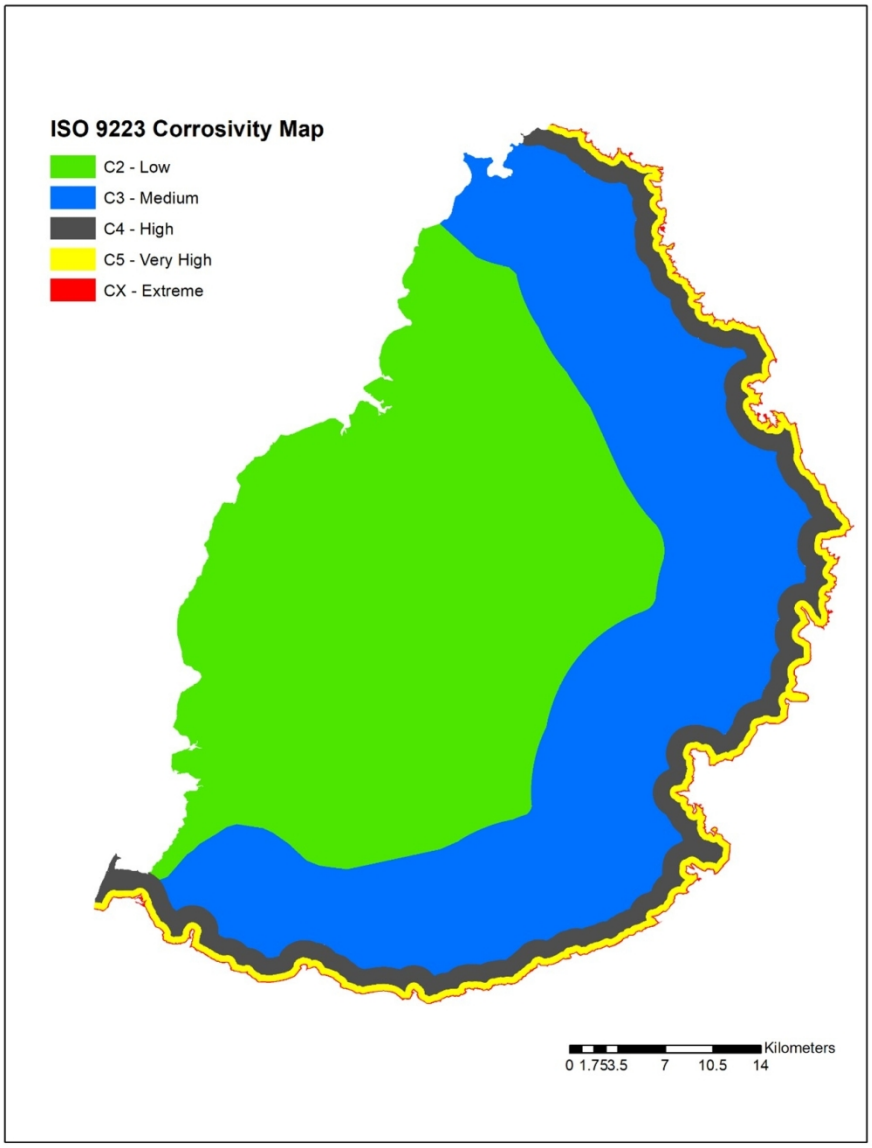


Figure 5. Preliminary corrosion map generated as a vector data model based on chloride deposition rate variation with distance from the east/south coastlines.

159x206mm (220 x 220 DPI)


Figure 6. Corrosion map generated as a vector data model, showing the most aggressive area in Port-Louis around 200 m downwind of Fort George Power Station.

95x123mm (220 x 220 DPI)

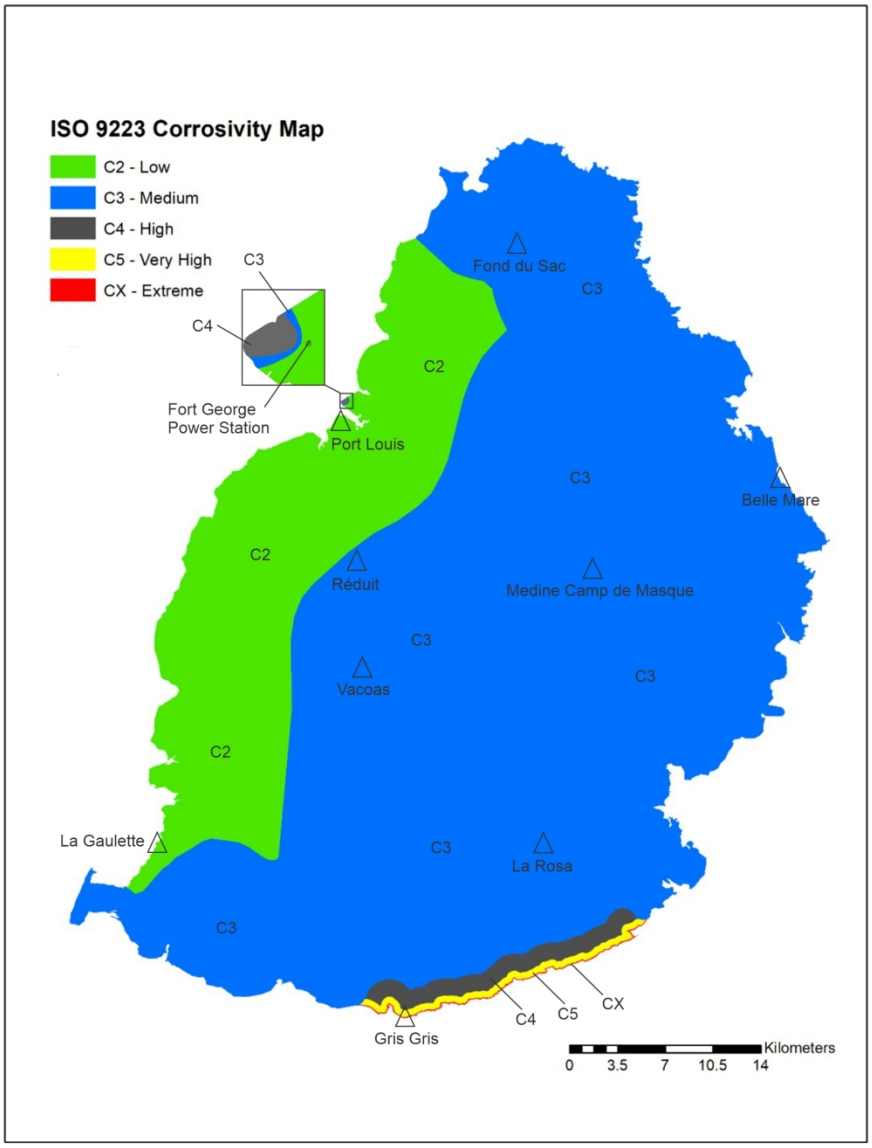


Figure 7. Corrosion map of Mauritius generated as a vector data model under consideration of the variation in surf-produced aerosol along the east and south coasts, high RH in central regions and $SO_2$ pollution in PL.

159x206mm (300 x 300 DPI)